Weiliang Kong, Zhaochong Zhang, Zhiguo Cheng, Bingxiang Liu, M. Santosh, Bowen Wei, Shan Ke, Lijuan Xu, and Xingchao Zhang, 2021, Mantle source of tephritic porphyry in the Tarim Large Igneous Province constrained from Mg, Zn, Sr, and Nd isotope systematics: Implications for deep carbon cycling: GSA Bulletin, https://doi.org/10.1130/B35902.1.

Supplemental Material

Figure S1. Field photographs of Wajilitag tephritic dykes.

Figure S2. Photomicrographs of the Wajilitag tephritic dykes.

Figure S3. LOI versus $\delta^{66}Zn$ for the Wajilitag tephritic porphyry.

Figure S4. (A) $\delta^{66}Zn$ versus Cr diagram. (B) $\delta^{66}Zn$ versus Ni diagram. (C) $\delta^{66}Zn$ versus MgO diagram. (D) $\delta^{66}Zn$ versus TiO_2 diagram.

Table S1. Major (wt%) and trace (ppm) elements of the Wajilitag tephritic porphyry, TLIP, NW China.

Table S2. Sr and Nd isotopic compositions of the Wajilitag tephritic porphyry, TLIP, NW China.

Table S3. Mg isotopic compositions of the Wajilitag tephritic porphyry, TLIP, NW China.

Table S4. Zn isotopic compositions of the Wajilitag tephritic porphyry, TLIP, NW China.

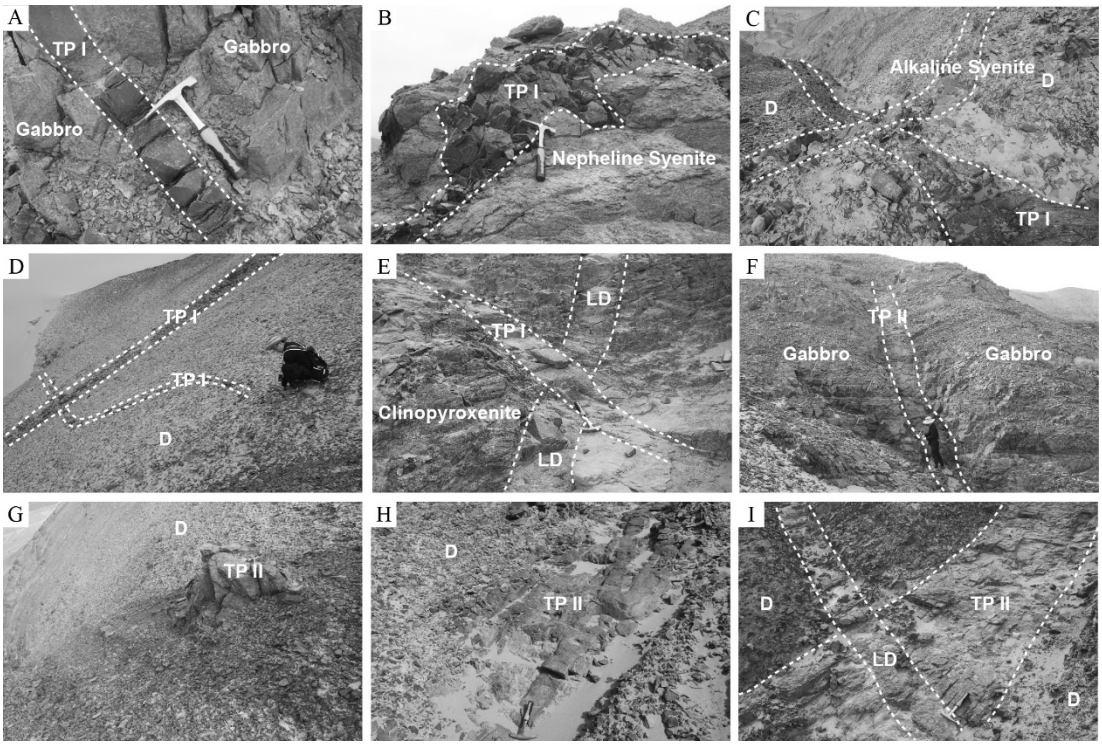

Figure S1. Field photographs of Wajilitag tephritic dykes. (A) Photograph showing the intrusion of tephritic porphyry I into the gabbro. (B) The tephritic porphyry I intrudes into nepheline syenites. (C) The tephritic porphyry I is cut by the later alkaline syenite dyke. (D) The tephritic porphyry is cut by another tephritic porphyry. (E) Photograph showing the intrusion of tephritic porphyry I into clinopyroxenite, and cutting the early lamprophyric dyke. (F) The tephritic porphyry II intrudes into the gabbro. (G) (H) The tephritic porphyry II intrudes into the Devonian strata. (I) The tephritic porphyry II is cut by later lamprophyric dyke. TP I: tephritic porphyry I; TP II: tephritic porphyry II; LD: lamprophyric dyke; D: devonian strata.

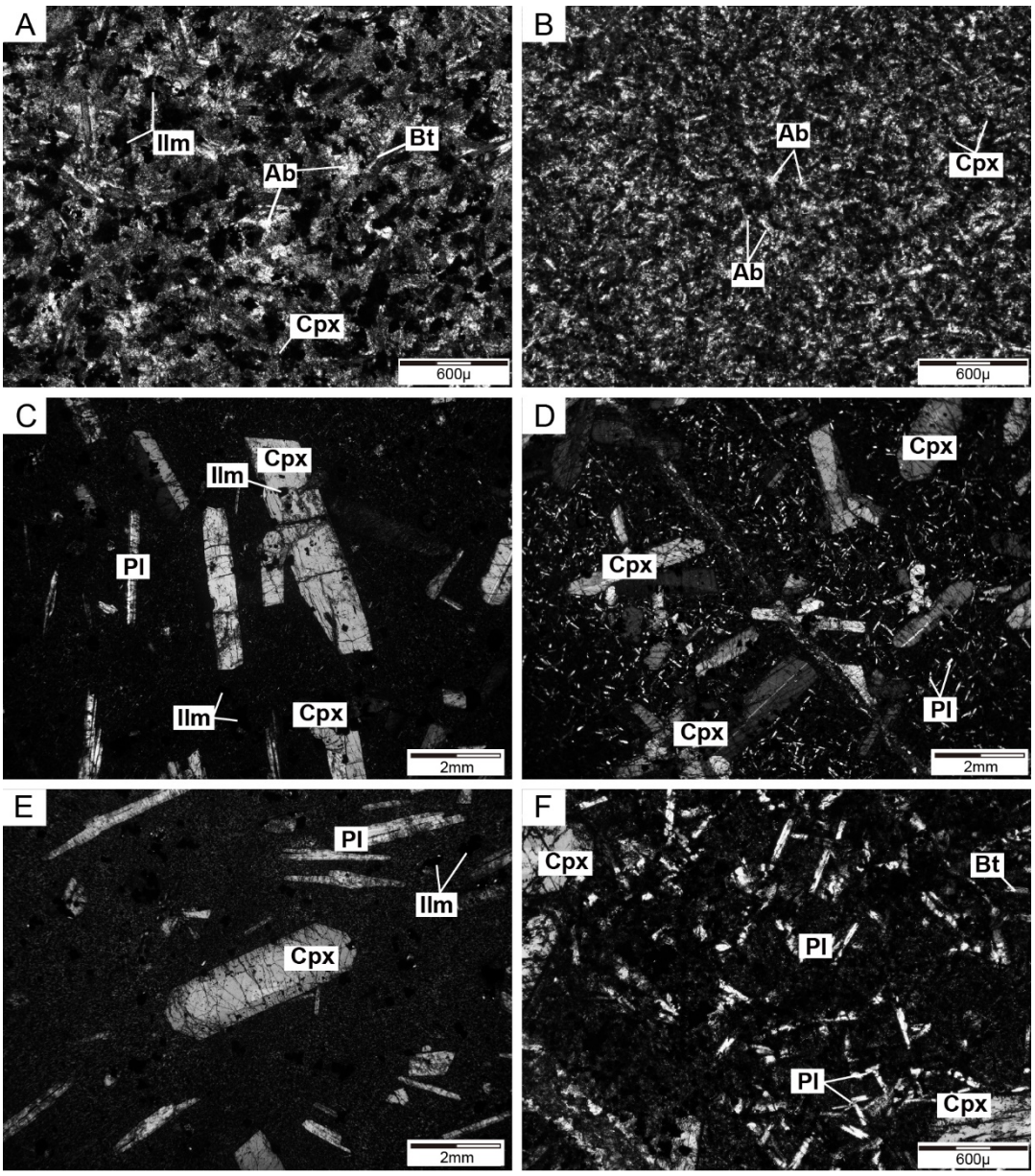

Figure S2. Photomicrographs of the Wajilitag tephritic dykes. (A–B) Tephritic porphyry I composed of albite, clinopyroxene, ilmenite and biotite. (C) Porphyritic texture of the tephritic porphyry II, crossed polarized light. (D) The clinopyroxene phenocrysts in the tephritic porphyry II, crossed polarized light. (E) The plagioclase occurring as phenocryst in the tephritic porphyry II, plane polarized light. (F) The groundmass of tephritic porphyry II comprising plagioclase, clinopyroxene, ilmenite and miner biotite, plane polarized light. Ab: albite, Ilm: ilmenite, Pl: plagioclase, Cpx: clinopyroxene, Bt: biotite.

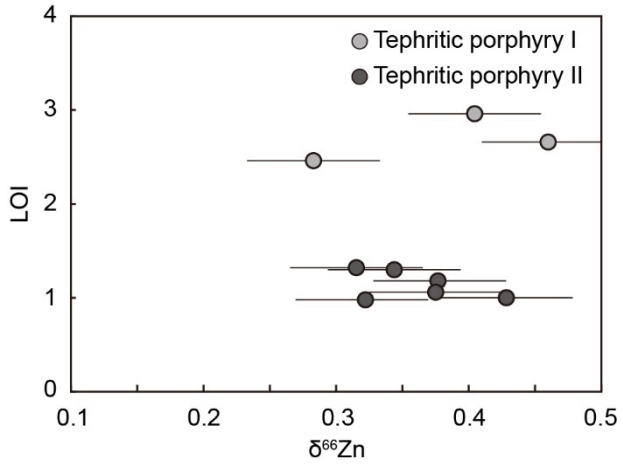

Figure S3. LOI versus $\delta^{66}Zn$ for the Wajilitag tephritic porphyry.

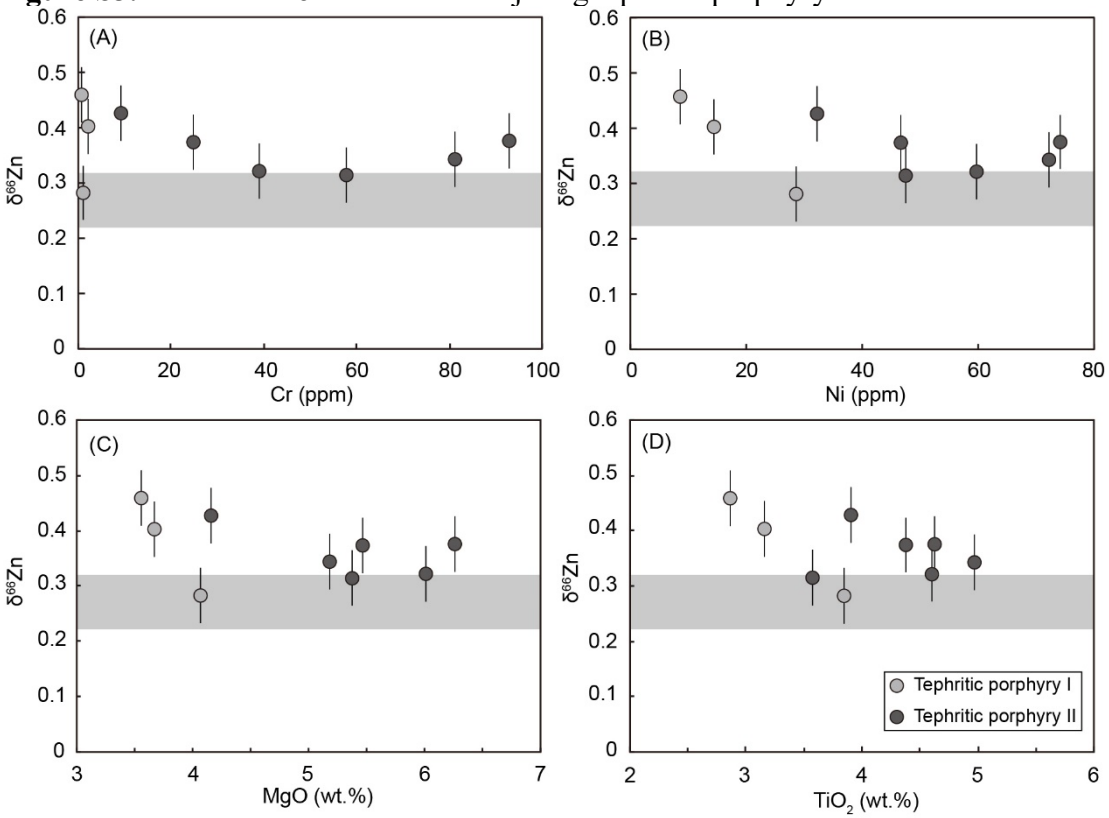

Figure S4. (A) $\delta^{66}Zn$ versus Cr diagram. (B) $\delta^{66}Zn$ versus Ni diagram. (C) $\delta^{66}Zn$ versus MgO diagram. (D) $\delta^{66}Zn$ versus TiO_2 diagram. The gray band represents the average $\delta^{66}Zn$ of the MORB (+0.27‰ ± 0.05‰, Wang et al., 2017 and Huang et al., 2018).

REFERENCES CITED

Huang, J., Zhang, X.C., Chen, S., Tang, L., Wörner, G., Yu, H., and Huang, F., 2018, Zinc isotopic systematics of Kamchatka-Aleutian arc magmas controlled by mantle melting: Geochimica et Cosmochimica Acta, v. 238, p. 85–101, https://doi.org/10.1016/j.gca.2018.07.012.

Wang, Z.Z., Liu, S.A., Liu, J., Huang, J., Xiao, Y., Chu, Z.Y., Zhao, X.M., and Tang, L.M., 2017, Zinc isotope fractionation during mantle melting and constraints on the Zn isotope composition of Earth's upper mantle: Geochimica et Cosmochimica Acta, v. 198, p. 151–167, https://doi.org/10.1016/j.gca.2016.11.014.